CrossMark

Structure, optical properties and photocatalysis performance of Cu$_2$O microspheres prepared by hydrothermal method

Xishun Jiang[1] · Zhongwei Li[1] · Qibin Lin[1] · Kexiu Dong[1] · Yangyi Zhang[1] · Zhaoqi Sun[2]

Abstract Cu$_2$O microspheres have been prepared by means of hydrothermal method as a function of reaction temperature ranging from 70 to 130 °C. Microstructure, morphology, chemical composition, optical properties and photocatalysis performance of the as-received samples were investigated in detail. X-ray diffraction analysis shows that Cu$_2$O and metal Cu content increase with increasing the reaction temperature. The samples are mainly composed of spherical particles and few Cu$_2$O with octahedral structure emerges at 110 and 130 °C. X-ray photoelectron spectroscopy measurement indicates that the surface atom ratio of Cu and O is estimated about 2.3:1 for the sample prepared at 110 °C. UV–visible absorption spectra show that absorption edge appears red shift with the increase in the reaction temperature and the absorption intensity at the same time. After illuminated for 100 min, the decolorization rates of the samples obtained at 110 and 130 °C are above 80 %.

1 Introduction

Cuprous oxide (Cu$_2$O) is a typical semiconductor material, which can be stimulated by visible light [1–4]. Its forbidden band gap is about 2.17 eV. The physical and chemical properties of Cu$_2$O are closely related to its morphology and particle size. Cu$_2$O is found as powder by artificial synthesis [5–8]. Because of the different synthetic methods and particle size, Cu$_2$O will appear red, orange, yellow, purple and other colors [9, 10]. Cu$_2$O has important applications in solar conversion battery and light catalytic due to its special semiconductor optoelectronic properties [11–13]. Cu$_2$O is a good coating additives, it has good prospect of application in ship antifouling paint, avoid water erosion and fade etc. Cu$_2$O can be prepared by a lot of methods, but hydrothermal method with low cost, simple synthesis conditions, the advantages of morphology and become one of the preferred technology to obtain Cu$_2$O [14–18]. Under hydrothermal conditions, the form of Cu$_2$O crystals are round-likely roundness cubes, octahedral, cube, rhombic dodecahedron and combination of pentagonal dodecahedron [19–21].

In this work, Cu$_2$O microspheres with different reaction temperatures were prepared by hydrothermal method under alkaline condition. The microstructure, surface morphology, chemical composition, the optical properties and photocatalysis performance were investigated using X-ray diffractometer (XRD), scanning electron microscope (SEM), X-ray photoelectron spectrometer (XPS) and ultraviolet–visible spectrophotometer (UV–Vis).

2 Experimental

The Cu$_2$O powder was prepared by hydrothermal method. The main chemical reagents required for the experiment are CuSO$_4$·5H$_2$O, NaOH, CH$_3$CH$_2$OH, CH$_3$COCH$_3$. Firstly, CuSO$_4$ solution (1.5 mol/L) and glucose solution (1.8 mol/L) were prepared, respectively. Then 10 mL CuSO$_4$ solution was poured into a beaker acting as the base

✉ Xishun Jiang
jxs915@126.com

✉ Zhaoqi Sun
szq@ahu.edu.cn

1 School of Mechanical and Electronic Engineering, Chuzhou University, Chuzhou 239000, China

2 School of Physics and Material Science, Anhui University, Hefei 230601, China

solution, and at the same time 10 mL NaOH solution was added into the previous solution. The beaker was constantly sonicated in an ultrasonic washer until the mixed solution was completely dissolved. After that, 10 mL glucose solution was added into the mixed solution. After ultrasonic oscillation in beaker, the solution was transferred into the PTFE-lined stainless autoclave. Repeat the above operation, and put the reaction kettle into the constant temperature box. The temperature is controlled at 70, 90, 110 and 130 °C, respectively and the heating time is 2.5 h. When the reaction was completed, we take out them from the stainless autoclave after cooling to room temperature. Then the samples were washed several times with deionized water and anhydrous ethanol. Finally, the samples were dried at 60 °C in air. After cooling to room temperature, the color of the samples in different reaction temperature show very great difference. The dominant color of the solution is green and dark green when the reaction is 70 and 90 °C. It shows a lot of Cu^{2+} was not involved in the reaction. But the color of solution after the reaction in 110 and 130 °C present light green, it shows only a small amount Cu^{2+} are still in solution. Finally the products turn to orange after washing and dry cleaning.

The crystal structure of the samples were analyzed by Japan-made Rigako D/Max-2200PC X-ray diffraction with Cu K_α radiation source and λ is 0.15418 nm, The pressure drop is 40 kV and the electricity is 40 mA. The surface morphology of the samples was characterized by scanning electron microscopy (SEM, S4800). Optional absorption studies were carried out employing a visible UV-2500 spectrophotometer.

3 Results and conclusion

3.1 Crystal structure analysis

Figure 1 shows the XRD patterns of Cu_2O prepared at different temperatures for 2.5 h. From Fig. 1, we can find the main diffraction peaks of the sample in higher reaction temperature are belonged to the cubic crystal system Cu_2O crystal. The peaks with 2θ values of 29.62°, 36.51°, 42.34° and 61.46° corresponding to (110), (111), (200), and (220) crystalplanes, respectively, are assigned as the pure Cu_2O (JCPDS: 05-0667) [22]. The peaks with 2θ values of 43.35° and 50.55° diffraction peak are belonged to metal Cu (111) and (200) crystal plane (JCPDS: 03-1015), respectively [23]. In the process of preparing the product, Cu^{2+} is reduced into Cu^+ by glucose and hydrolysis can generate Cu_2O in the presence of alkali.

The average crystallite size of Cu_2O can be estimated by Scherrer equation [24].
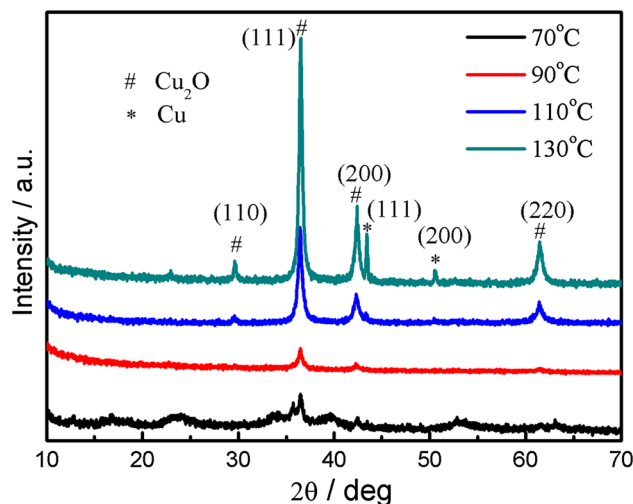

Fig. 1 X-ray diffraction patterns for the Cu_2O films

$$D = \frac{K\lambda}{\beta \cos \theta} \tag{1}$$

Here, D is average crystallite size, K is a constant (0.9), λ is the wavelength of CuK_α radiation (0.15418 nm), β is full width at half maximum of peak and θ is the diffraction angle. The estimated results were listed in Table 1. With the increase in the reaction temperature, the average crystallite size of the microspheres increases which can be due to a large amount of Cu_2O crystal nucleus obtained at higher reaction temperature.

Based on Fig. 1 and Table 1, the sample prepared at 130 °C show the strongest diffraction intensity. By analyzing diffraction peak intensity and half peak width of Cu_2O (111) crystal plane, we conclude that Cu_2O crystal shows the tendency of increase with the increase of reaction temperature. And when the reaction temperature is 110 °C, XRD showed Cu diffraction peaks are very weak in the product, while the product is consisted of Cu_2O and Cu at 130 °C. The higher reaction temperature is, the better Cu_2O crystal performance is. But at the same time, metal Cu content increases. In order to obtain pure and high-crystallization cuprous oxide, the reaction temperature is controlled at 110 °C.

Table 1 Average crystallite size of Cu_2O (111) crystal plane for different reaction temperatures

| Reaction temperature (°C)	Average crystallite size (nm)
70	19.7
90	28.9
110	75.6
130	95.3

3.2 Surface morphology analysis

The morphology of the samples prepared for different reaction temperatures investigated by SEM is shown in Fig. 2. Figures 2e, f are the magnified graphs for the samples deposited at 110 and 130 °C, respectively. The surface morphology of the samples depends on the reaction temperature. The samples prepared at 70 and 90 °C exhibit sedimentary and irregular morphology as shown in Fig. 2a, b. XRD analysis found the two samples contain more impurities. It is mentioned that serious phenomenon of reunion is emerged when the reaction temperature rises to 90 °C (Fig. 2b). Figure 2c, d illustrated that the samples are mainly composed of morphology spherical particles and very small amounts of Cu_2O with octahedral structure are emerged when the reaction temperatures are 110 and 130 °C. The average grain size of Cu_2O is about 1-3 μm when the reaction temperature is 110 °C. When the

reaction temperature is 130 °C, Cu_2O crystal grain size is larger and distribution between 2 and 4 μm. From the Fig. 2e, f, the Cu_2O particles increased significantly as the reaction temperature. In addition, with increasing reaction temperature Cu_2O have some phenomenon of reunion, and particle morphology from round-likely roundness cubes to part of octahedral. Figure 3 presents TEM images of Cu_2O microspheres prepared at 110 °C. SEM and TEM results are in good accordance with previous XRD analysis.

3.3 XPS analysis

In order to investigate the composition and chemical state, X-ray photoelectron spectroscopy (XPS) has been carried out for the samples obtained at different temperatures. The XPS survey spectrum is shown in Fig. 4a. The adventitious C1s peak was calibrated at 285 eV and used as an internal standard to compensate for any charging effects. Figure 4b,
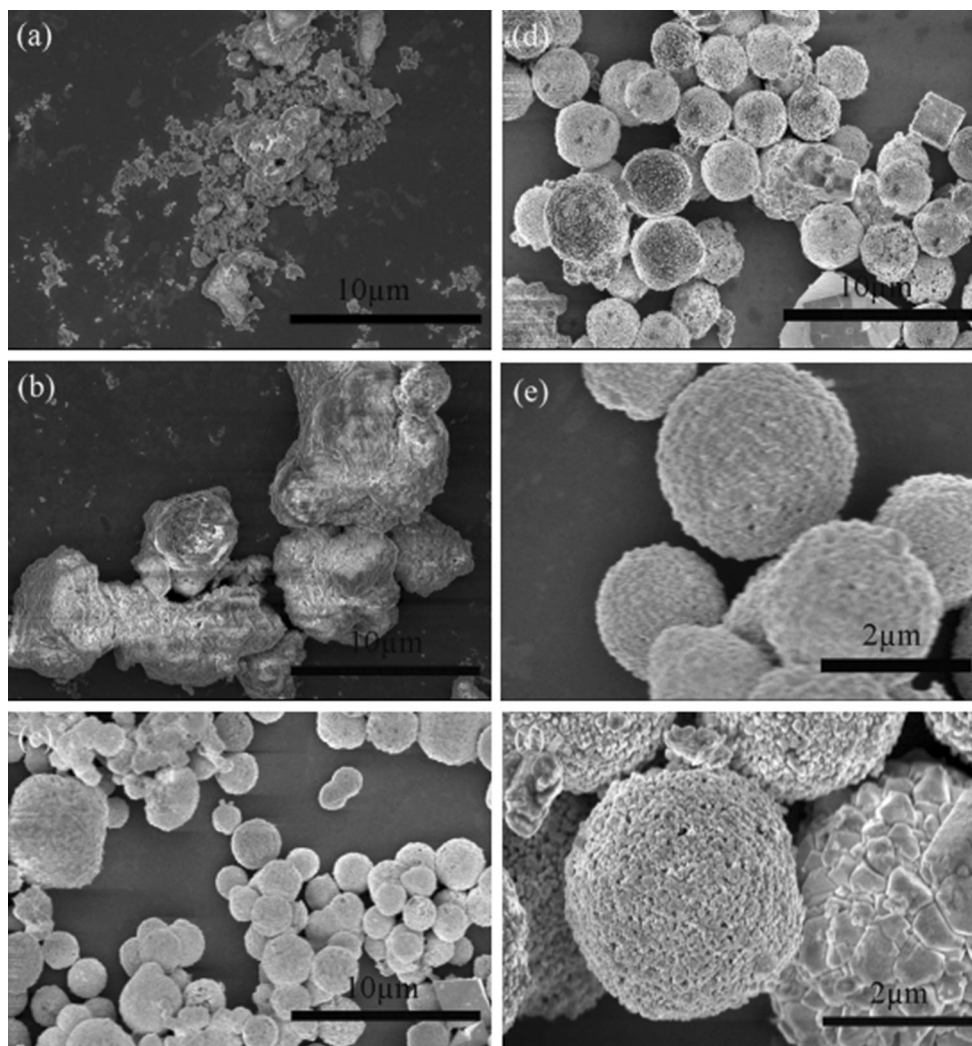
Fig. 2 SEM images of the samples **a** 70 °C, **b** 90 °C, **c** 110 °C, **d** 130 °C
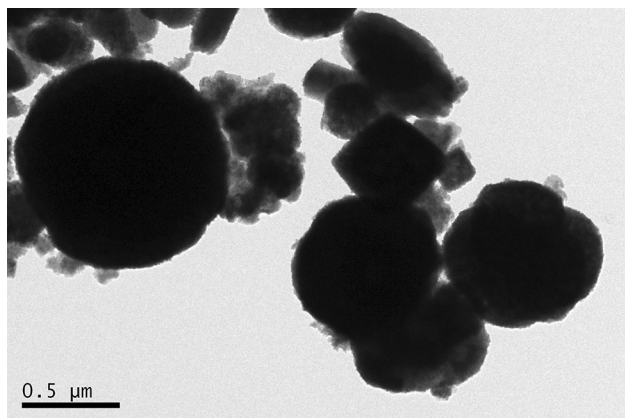
Fig. 3 TEM image of the sample deposited at 110 °C

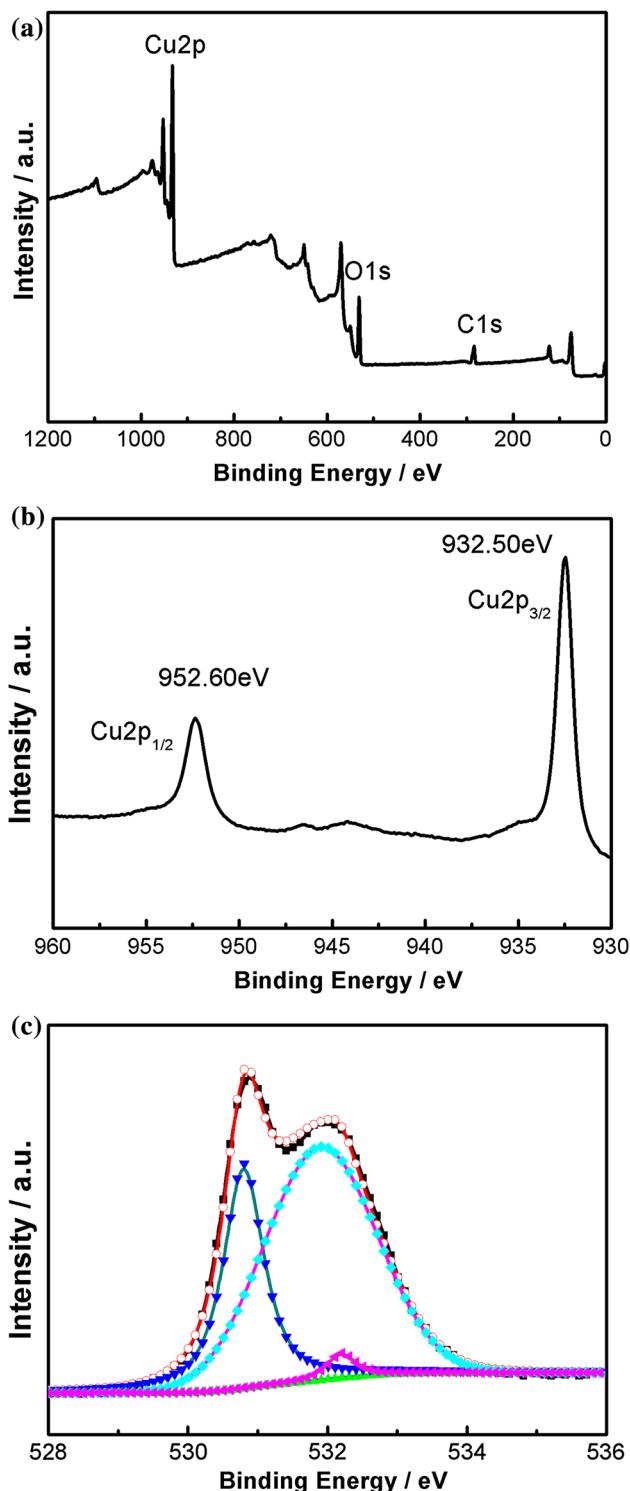**Fig. 4** XPS spectra of the sample deposited at 110 °C **a** survey spectrum, **b** Cu2p and **c** O1s

c show the core-level spectra of Cu2p and O1s of the sample obtained at 110 °C. In the spectrum of Cu2p, both the Cu2p3/2 (932.50 eV) and Cu 2p1/2 (952.60 eV) peaks can be characterized as Cu_2O or Cu [25, 26]. Between 935.0 and 950.0 eV appeared extremely weak satellite peaks, indicating that the surface of the deposited film is not oxidized in air. Figure 4b shows photoelectron spectroscopy peak of O1s can be fitted to three peaks. The peak position of 530.8 eV is oxygen of Cu_2O, while the peak position of 531.9 eV and the peak position of 532.2 eV represent oxygen of OH groups and oxygen of the surface adsorption, respectively [27]. The Cu and O surface atom ratio of the sample is estimated about 2.3:1.

3.4 UV–Vis absorption

The UV–Vis absorption spectra of the samples are shown in Fig. 5. From Fig. 5, ultraviolet visible absorption of the samples obtained at different temperatures reveals obvious difference. It cannot make a corresponding quantitative analysis from the measured absorption spectrum of the sample prepared at 70 °C due to its impurity. Under the corresponding temperature of 90 °C, Cu_2O in visible light absorption edge is not obvious for agglomeration and poor crystalline. Compared with the UV–visible absorption spectra of the samples prepared at 110 and 130 °C, absorption edge appears red shift phenomenon with reaction temperature increasing and the absorption intensity enhances at the same time. The sample obtained at 130 °C can absorb longer wavelength light due to its fewer particle number and larger particle size. So it minimizes light scattering and will be beneficial to improve the photocatalytic activity.

3.5 Photocatalytic degradation of MO

The photocatalytic activities of the products were carried out by the degradation of MO solution under visible light irradiation. The photocatalytic activity was tested under simulated sunlight AM1.5 (10 mW/cm^2). 0.1 g of the synthetic samples was put into the beakers and 10 mg L^{-1} MO solutions with the volume 20 mL were added into the
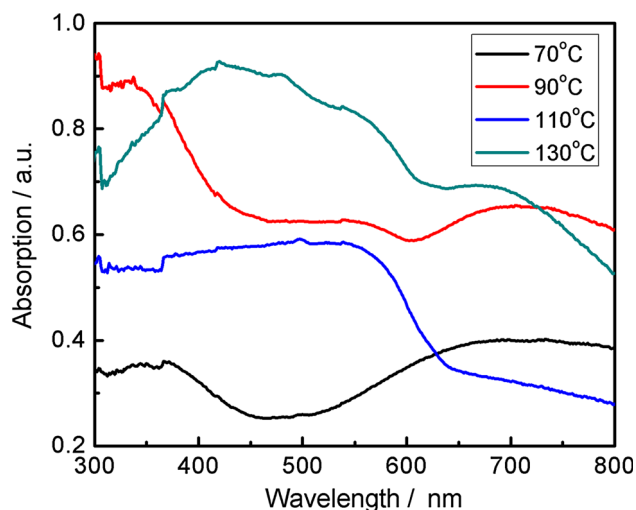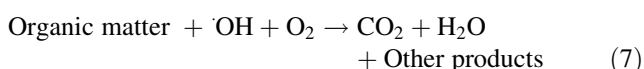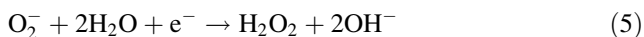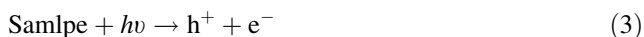
Fig. 5 UV–Vis absorption spectra of the samples deposited for different temperatures

beakers. The UV–visible absorption spectra of the samples were recorded after 100 min. The experimental results are shown in Table 2. The photocatalytic properties of Cu_2O were characterized by decolorization rate (D) of MO [28].

$$D = \frac{A_0 - A}{A_0} \times 100\%$$ (2)

Here, A_0 and A are the absorbances of MO solution before and after irradiation. As indicated in Table 2, the products obtained at lower temperatures exhibit a weak ability of the degradation of MO. The poor degradation ability of the products can be ascribed to the fact that Cu_2O cannot be formed under low temperature. At the same conditions, the products obtained at 110 and 130 °C performed well in degrading MO.

During the degradation process, reactions listed below may be occurred [29].

$$\text{Samlpe} + h\upsilon \rightarrow \text{h}^+ + \text{e}^-$$ (3)

$$\text{e}^- + \text{O}_2 \rightarrow \text{O}_2^-$$ (4)

$$\text{O}_2^- + 2\text{H}_2\text{O} + \text{e}^- \rightarrow \text{H}_2\text{O}_2 + 2\text{OH}^-$$ (5)

$$\text{H}_2\text{O}_2 + \text{e}^- \rightarrow \cdot\text{OH} + \text{OH}^-$$ (6)

$$\text{Organic matter} + \cdot\text{OH} + \text{O}_2 \rightarrow \text{CO}_2 + \text{H}_2\text{O} + \text{Other products}$$ (7)

Table 2 Decoloration rate of MO at different reaction temperatures

Reaction temperature (°C)	Decoloration rate (%)
70	5.2
90	6.3
110	85.6
130	87.5

The visible light can provide energy to excite electrons from the valance band to the conduction band of Cu_2O and the holes still stay at lower valance band. Cu_2O have the capacity to absorb atomic oxygen and surface electrons of Cu_2O photocatalyst convert the adsorbed atomic oxygen to O_2^-. O_2^- act with water and electrons to produce H_2O_2 and hydroxyl radical $\cdot$OH. $\cdot$OH has a strong oxidant property and the organics in solution are oxidized to inorganic. The higher is separation efficiency of electron hole pairs of the sample, the better is photocatalytic effect. So the products obtained at 110 and 130 °C show excellent degradation of MO. After illuminated for 100 min, the decolorization rate of the samples is above 80 %.

4 Conclusions

In summary, cuprous oxide with different temperatures 70, 90, 110 and 130 °C were prepared using simple hydrothermal method with glucose as the reducing agent. Microstructure, surface morphology, chemical composition and optical properties of the deposited samples were investigated in detail. The main results are as follows:

1. The XRD results show that Cu^{2+} in the glucose solution can not be completely restored into Cu^+ at lower (70 and 90 °C) reaction temperature. The intensity of diffraction peaks belong to Cu_2O increase with increasing the reaction temperature.
2. With the increase of reaction temperature, Cu_2O crystal shows the tendency of increase. In addition, Cu_2O will appear agglomeration and particle morphology showed from round-likely roundness cubes to octahedral.
3. The average absorption coefficient of the samples prepared at 130 °C reaction temperature is larger than that deposited at 110 °C. The sample obtained at 130 °C can absorb longer wavelength light due to its fewer particle number and larger particle size.
4. The samples obtained at 110 and 130 °C show excellent degradation of MO. After illuminated for 100 min under visible light, the decolorization rate of the samples is above 80 %.

References

1. L. Hu, Y. Huang, F. Zhang, Q. Chen, Nanoscale **5**, 4186–4190 (2013)
2. F. Zhou, Z. Li, G.J. Shenoy, L. Li, H. Liu, ACS Nano **7**, 6939–6947 (2013)
3. W. Lee, Y.S. Lim, S. Kim, J. Jung, Y.K. Han, S. Yoon, L. Piaoe, S.H. Kim, J. Mater. Chem. **21**, 6928–6933 (2011)
4. S. Li, X. Ge, S. Jiang, X. Peng, Z. Zhang, W. Li, S. Yu, J. Mater. Sci. **50**, 4115–4121 (2015)
5. H. Azimi, S. Kuhri, A. Osvet, G. Matt, L.S. Khanzada, M. Lemmer, N.A. Luechinger, M.I. Larsson, E. Zeira, D.M. Guldi, C.J. Brabec, J. Am. Chem. Soc. **136**, 7233–7236 (2014)
6. C.S. Tan, S.C. Hsu, W.H. Ke, L.J. Chen, M.H. Huang, Nano Lett. **15**, 2155–2160 (2015)
7. M.D. Susman, Y. Feldman, A. Vaskevich, I. Rubinstein, ACS Nano **8**, 162–174 (2014)
8. K. Giannousi, G. Sarafidis, S. Mourdikoudis, A. Pantazaki, C. Dendrinou-Samara, Inorg. Chem. **53**, 9657–9666 (2014)
9. X. Yan, J. Yang, L. Ma, X. Tong, Y. Wang, G. Jin, X. Guo, J. Solid State Electrochem. **19**, 3195–3199 (2015)
10. L. Liu, W. Yang, Q. Li, S. Gao, J.K. Shang, A.C.S. Appl, Mater. Interfaces **6**, 5629–5639 (2014)
11. J. Wang, J. Ma, X. Li, Y. Li, G. Zhang, F. Zhang, X. Fan, Chem. Commun. **50**, 14237–14240 (2014)
12. H. Bao, Z. Zhang, Q. Hua, W. Huang, Langmuir **30**, 6427–6436 (2014)
13. D.Y. Kim, C.W. Kim, J.H. Sohn, K.J. Lee, M.H. Jung, M.G. Kim, Y.S. Kang, J. Phys, Chem. C **119**, 13350–13356 (2015)
14. P. Wang, X. Zhao, H. Li, L. Li, J. Li, G. Ma, J. Chang, RSC Adv. **4**, 37542–37546 (2014)
15. J. Kim, H.S. Kim, J.H. Choi, H. Jeon, Y. Yoon, J. Liu, J.G. Park, P.V. Braun, Chem. Mater. **26**, 7051–7058 (2014)
16. H. Zheng, L. Qin, H. Lin, M. Nie, Y. Li, Q. Li, J. Nanosci. Nanotechnol. **15**, 6063–6068 (2015)
17. C. Dong, H. Zhong, T. Kou, J. Frenzel, G. Eggeler, Z. Zhang, A.C.S. Appl, Mater. Interfaces **7**, 20215–20223 (2015)
18. Y. Zhao, L. Fan, Y. Zhang, H. Zhao, X. Li, Y. Li, L. Wen, Z. Yan, Z. Huo, A.C.S. Appl, Mater. Interfaces **7**, 16802–16812 (2015)
19. Y.H. Tsai, K. Chanda, Y.T. Chu, C.Y. Chiu, M.H. Huang, Nanoscale **6**, 8704–8709 (2014)
20. K. Tu, Q. Wang, A. Lu, L. Zhang, J. Phys. Chem. C **118**, 7202–7210 (2014)
21. Z. Zhai, X. Guo, Z. Jiao, G. Jin, X.Y. Guo, Catal. Sci. Technol. **4**, 4196–4199 (2014)
22. W.C. Huang, L.M. Lyu, Y.C. Yang, M.H. Huang, J. Am. Chem. Soc. **134**, 1261–1267 (2012)
23. C.W. Li, M.W. Kanan, J. Am. Chem. Soc. **134**, 7231–7234 (2012)
24. X. Jiang, Y. Zhang, Z. Li, Y. Ren, M. Zhang, G. He, X. Song, Z. Sun, J. Mater. Sci.: Mater. Electron. **26**, 2070–2075 (2015)
25. J. Dai, X.M. Fan, H. Liu, J. Wang, H.R. Liu, F.Z. Zhang, J. Nanosci. Nanotechnol. **12**, 6412–6419 (2012)
26. M.A. Mahmoud, W. Qian, M.A. El-Sayed, Nano Lett. **11**, 3285–3289 (2011)
27. I.N. Kholmanov, S.H. Domingues, H. Chou, X. Wang, C. Tan, J.Y. Kim, H. Li, R. Piner, A.J.G. Zarbin, R.S. Ruoff, ACS Nano **7**, 1811–1816 (2013)
28. J. Ma, K. Wang, L. Li, T. Zhang, Y. Kong, S. Komarneni, Ceram. Int. **41**, 2050–2056 (2015)
29. S. Li, X. Ge, S. Jiang, X. Peng, Z. Zhang, W. Li, S. Yu, J. Mater. Sci.: Mater. Electron. **50**, 4115–4121 (2015)